Editors' Suggestion

Quantitative assessment of the spatial crowding heterogeneity in cellular fluids

Claudia Donth and Matthias Weiss*

Experimental Physics I, University of Bayreuth, Universitätsstr. 30, D-95447 Bayreuth, Germany

(Received 10 January 2019; published 28 May 2019)

Mammalian cells are crowded with macromolecules, supramolecular complexes, and organelles, all of which equip intracellular fluids, e.g., the cytoplasm, with a dynamic and spatially heterogeneous occupied volume fraction. Diffusion in such fluids has been reported to be heterogeneous, i.e., even individual single-particle trajectories feature spatiotemporally varying transport characteristics. Complementing diffusion-based experiments, we have used here an imaging approach to assess the spatial heterogeneity of the nucleoplasm and the cytoplasm in living interphase cells. As a result, we find that the cytoplasm is more crowded and more heterogeneous than the nucleoplasm on several length scales. This phenomenon even persists in dividing cells, where the mitotic spindle region and its periphery form a contiguous fluid but remain nucleoplasmlike and cytoplasmlike, respectively.

DOI: 10.1103/PhysRevE.99.052415

I. INTRODUCTION

The interior of mammalian cells harbors a plethora of macromolecules, supramolecular complexes, and membrane-enclosed organelles that dynamically interact and reorganize on multiple timescales. While individual concentrations of specific molecules often are fairly low, cellular fluids like the cytosol are usually referred to as being crowded by macromolecules since their overall concentration is in the range of 100–500 mg/ml [1]. Beyond the molecular level, a variety of supramolecular clusters, granules, and membrane-enveloped structures, from tiny transport vesicles to whole organelles, equip the cytoplasm with an additional nontrivial architecture [2], highlighting that cytoplasmic crowding needs to be viewed as a multiscale phenomenon. A similar complexity is also observed in the nucleoplasm where several membraneless organelles, e.g., nucleoli and Cajal bodies, are embedded in a protein-rich fluid that hosts the hierarchically folded DNA [2]. Hence, in both cases a wide range of sizes of crowders, from few nanometers up to microns, can be expected to create a locally varying occupied volume fraction that significantly impacts on the physical properties of and transport within cellular fluids.

Indeed, slowed-down and even subdiffusive transport characteristics have been reported frequently for crowded intracellular fluids on submicron length scales (see, for example, [3–5] for reviews). Most studies have, for simplicity, neglected the complex multiscale architecture of cytoplasm and nucleoplasm, and reported mean values of diffusion coefficients or anomaly exponents with all spatial heterogeneity being integrated into the observable's error bars. Yet, averaging over data gathered from different loci inside a cell tacitly assumes the effects of crowding, and hence the crowding itself, to be homogeneous. Given the complex architecture of the cell, this assumption appears questionable.

In accordance with this caveat, recent studies have reported on the observation of a diffusion heterogeneity in biological and biomimetic fluids [6–8], i.e., an apparent change of diffusion coefficients even within single-particle trajectories. Moreover, spatial variations in diffusion maps have been reported for culture cells [9] and for the early embryo of *Caenorhabditis elegans* [10]. Local diffusion measurements and fluorescence lifetime analysis of a molecular rotor dye have furthermore suggested that nanoscale and mesoscale variations in the apparent occupied volume fraction are significantly higher in cellular fluids than in biomimetic media [11]. These findings strongly support the notion that spatial inhomogeneities impact on intracellular transport behavior. Yet, data on the multiscale heterogeneity of cellular fluids, independent of transport measurements, are scarce.

In order to close this gap, we have focused here on elucidating the spatial heterogeneity of the crowded cytoplasm and nucleoplasm via a simple imaging approach. In particular, we show that nucleoplasm and cytoplasm of HeLa cells display significant differences in their average occupied volume fraction and in their local heterogeneities. These differences even persist after nuclear envelope breakdown, i.e., when the previously distinct nucleoplasm and cytoplasm form a single contiguous fluid during cell division. Reporting only on the effective excluded volume of the compartments, our data show similarities but also differences to previous studies that elucidated the spatial crowding heterogeneity via diffusion measurements.

II. MATERIALS AND METHODS

A. Sample preparation and imaging

HeLa cells were cultured in Dulbecco's Minimal Essential Medium (Invitrogen), supplemented with 10% fetal calf serum (Biochrom), 1% L-glutamine (Invitrogen), 1% sodium pyruvate (Invitrogen), and 1% penicillin/streptomycin (Invitrogen). Cells were incubated at 37 °C in a 5% CO_2 atmosphere. For microscopy, cells were cultured on μ-slide microscopy chambers (ibiTreat, two well; Ibidi), supplemented with transparent imaging medium (MEM without phenol-red, enriched with 5% fetal calf serum and 50 mM HEPES).

*Corresponding author: matthias.weiss@uni-bayreuth.de

Transient transfection with a low-expression plasmid for enhanced green fluorescent protein (EGFP) as described before [12] was performed using either PeqFECT (Peqlab) or Fugene6 (Promega) according to the manufacturer's protocols (2 μl Pecfect or 3 μl Fugene6, 1 μg DNA in 100 μl supplement-free Opti-MEM GlutaMAX medium from Gibco). For measurements in metaphase, cells were synchronized for 12 h in the presence of 50 nM nocodazole (Sigma) as described before [12]. Prior to microscopy, synchronized cells were washed with PBS and incubated with culture medium at 37 °C for 30 min.

Imaging was performed with a Leica SP5-TCSPC confocal laser scanning microscope using a 63×/1.2NA water immersion objective (Leica Microsystems, Mannheim, Germany). All experiments were performed at 37 °C using a custom-made incubator chamber. Samples were illuminated at 488 nm and fluorescence was detected in the range 500–550 nm. Image acquisition was designed to meet the Nyquist criterion and respecting the diffraction limit. The pinhole was set to one Airy unit throughout, i.e., every pixel in an image corresponded to a diffraction-limited volume ("voxel"). Images of metaphase (interphase) cells were taken with 512 × 512 (1024 × 1024) pixels [pixel size 100.31 nm (100.21 nm)] using monodirectional scanning at a frequency of 200 Hz (100 Hz), resulting in a pixel dwell time of 9.76 μs. Neither averaging nor smoothing was used in any measurement. For quality control, i.e., to explore the impact of potential variations in the microscope's performance and possible temporal variations in crowding levels, some cells were repeatedly imaged under the same illumination and detection settings. No significant changes in the results were observed. Zoomed areas were adjusted such that the pixel size was preserved. Laser power and detector settings were adjusted to exploit the dynamic range of the photomultipliers without saturation effects. Representative images are shown in Figs. 1(a) and 1(b).

Dye solutions of Alexa488 (ThermoFisher) in MilliQ water at varying concentrations were prepared immediately before measurements and imaged at the same conditions as interphase cells.

To quantify the heterogeneity of the cellular fluorescence intensity, several regions of interest (ROIs) were selected in the nucleoplasm and in the cytoplasm of each interphase cell (in metaphase: in the periphery and in the spindle region); these cellular compartments could be discriminated easily in transmission images. For each ROI the mean and the variance of the ROI's pixel-wise fluorescence values were determined and used for further analysis (see main text and also next subsection). All image analysis steps were done with custom-written MATLAB codes.

B. Image analysis

In an idealized imaging situation, the number of fluorescence photons k obtained for each voxel in a homogeneous sample is given by a Poissonian

$$p(k,\lambda) = \frac{\lambda^k}{k!} e^{-\lambda} \tag{1}$$

with $\langle k \rangle = \lambda$ being the mean photon number and $\sigma^2(k) = \langle (k - \langle k \rangle)^2 \rangle = \lambda$ denoting the variance. In the linear response regime, the mean number of photons obtained for a voxel is determined by the average number of dye molecules in each voxel $\langle N \rangle$, their quantum yield, and the illumination intensity, i.e., $\lambda \propto \langle N \rangle$.

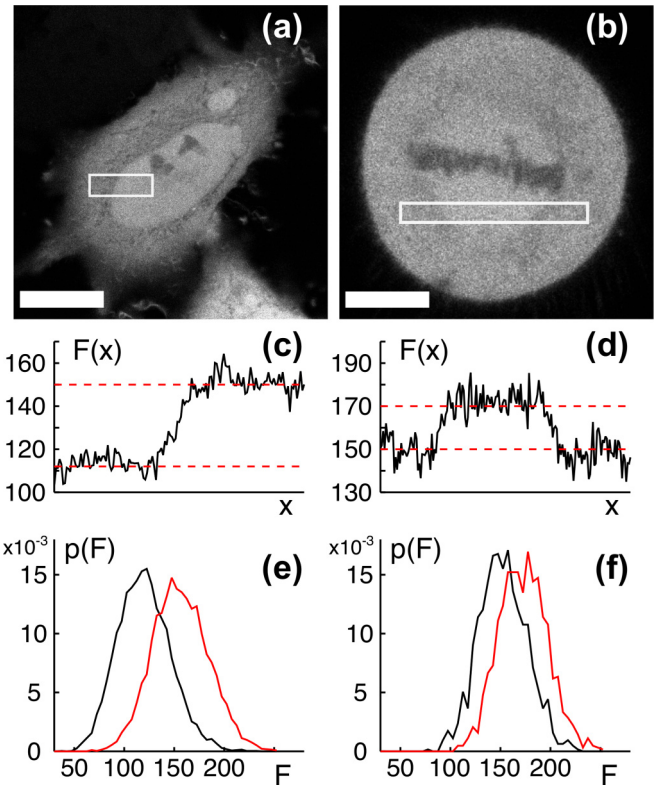

FIG. 1. Representative fluorescence images of HeLa cells expressing free EGFP (a) in interphase (750 × 750 pixels, scale bar: 10 μm), and (b) in metaphase (300 × 300 pixels, scale bar: 4 μm). Indicated rectangles (150 × 40 and 180 × 20 pixels, respectively) were used for an averaged fluorescence profile $F(x)$ along the horizontal direction x. (c) In interphase, the fluorescence profile $F(x)$ shows a roughly 30% higher mean in the nucleus than the cytoplasm (indicated by dashed lines). (d) A smaller but still significant increase in the fluorescence (about 15%) is seen in metaphase when crossing the mitotic spindle region. (e) An elevated fluorescence in the nucleus (red) as compared to the cytoplasm (black) is also seen in the probability distribution function of voxel-wise fluorescence values $p(F)$. (f) A similar result is found when comparing $p(F)$ from the mitotic spindle region (red) versus its periphery (black).

Experimentally, the hallmark of Eq. (1), i.e., the equivalence of the mean and the variance, is not observed due to an imperfect photon detection and a detector-dependent translation to discrete fluorescence intensity values n. In particular, the variance is larger than the mean (see Fig. 2 for an example). Nonetheless, the variance remains proportional to the mean with a prefactor that is clearly larger than unity and that depends on the detector settings (see Fig. 2, inset). Starting from the ideal case, this experimental finding can be modeled via a simple mapping $n = \beta(k - \langle k \rangle) + \langle k \rangle$, that leaves the mean unchanged, $\langle n \rangle = \langle k \rangle = \lambda$, but stretches the variance by a factor β^2, i.e., $\sigma^2(n) = \langle (n - \langle n \rangle)^2 \rangle = \beta^2 \lambda$. Indeed, this mapping captures well the experimentally observed

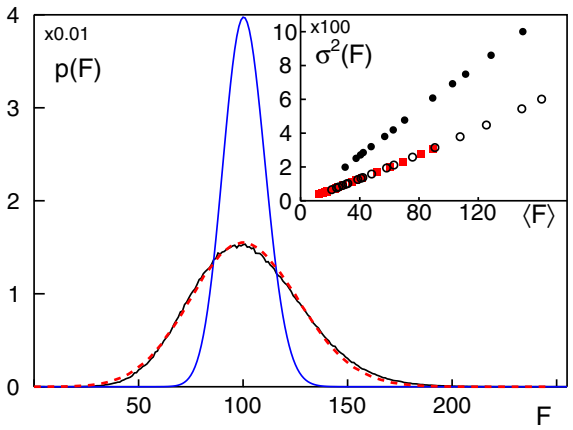

FIG. 2. The probability distribution function of voxel-wise fluorescence values $p(F)$ obtained from a homogeneous dye solution (black) is broader than a Poissonian with the same mean value (blue). The overdispersion can be modeled by a customized mapping that preserves the mean but increases the variance of fluorescence values (see main text for details), eventually yielding a very good fit to the data (red dashed line). Inset: a linear relation between the mean fluorescence $\langle F\rangle$ and the variance $\sigma^2(F)$ is observed for homogeneous samples. Varying the dye concentration and illumination intensity at fixed detector settings (photomultiplier voltage: 800 V) does not change the prefactor (black circles and filled red squares). Yet, changing detector settings (to 900 V) increases the prefactor (filled black circles), leading to larger variances at the same mean. Please note the scale factor at both plots.

distribution of fluorescence values (see Fig. 2 for an example) as long as $\lambda \gg \beta^2$.

For inhomogeneous samples, spatial fluctuations in the accessible volume fraction φ (the complement of the occupied volume fraction) on length scales below the diffraction limit are reflected by changes in the average number of fluorescent particles per voxel $\langle N\rangle \propto \varphi$. Therefore, also the voxels' mean fluorescence value $\lambda = A\varphi \propto \langle N\rangle$ shows spatial variations, with the prefactor A encoding all proportionality constants. Assuming for simplicity that the accessible volume fraction follows a Gaussian probability distribution function (PDF) with mean φ_0 and variance $\sigma^2(\varphi) \ll \varphi_0^2$ yields a Gaussian PDF also for λ, with mean and variance being $\langle\lambda\rangle = A\varphi_0$ and $\sigma^2(\lambda) = A\sigma^2(\varphi)$, respectively. Using the Gaussian PDF for λ to consider spatial variations of the accessible volume fraction in Eq. (1) and applying the mapping $k \to n$ to capture the detection process updates the mean and the variance of voxel-wise fluorescence values to $\langle n\rangle = A\varphi_0$ and $\sigma^2(n) = \beta^2[A\varphi_0 + A^2\sigma^2(\varphi)]$, respectively. Both expressions are used below to assess the region-wise and voxel-wise heterogeneity of the accessible volume fraction in intracellular fluids.

III. RESULTS AND DISCUSSION

To assess the heterogeneity of biological fluids by simple imaging, i.e., to explore their varying extent of excluded volumes, we have focused on three different length scales: On the largest length scale, we have exploited compartment-specific mean fluorescence values to compare the average accessible volume fraction. On intermediate and small length scales, we rather compared fluctuations of the apparent accessible volume fraction within each compartment by exploiting the statistics of fluorescence values. Due to the different evaluation approaches, we have summarized our findings in two sections.

A. Spatial heterogeneity between compartments

A first and straightforward impression of the multiscale heterogeneous crowdedness in mammalian cells during interphase is obtained when inspecting fluorescence images after transient transfection with free EGFP (Fig. 1). Due to the presence of various supramolecular and organellelike structures in the cytoplasm, the nanosized EGFP molecules appear to be excluded from a variety of subvolumes, equipping the cytoplasmic fluorescence with a patchy pattern [Fig. 1(a)]. In contrast, the nucleoplasmic fluorescence looks rather homogeneous and is much less speckled (apart from very few loci that are occupied by dense nuclear bodies like nucleoli). Interestingly, the average nucleoplasmic fluorescence seemed markedly higher than the cytoplasmic signal in almost all cells. Moreover, when imaging the same cell repeatedly over a period of 1 h, no significant change in this difference in fluorescence intensities was observed. This qualitative impression is quantitatively confirmed by an averaged fluorescence profile across both compartments [Fig. 1(c)]: on average, the nucleoplasmic signal is about 30% higher than its cytoplasmic counterpart. This finding is further substantiated by the compartment-specific probability distribution function (PDF) of voxel-wise fluorescence values $p(F)$, for which a significantly larger mean is seen for data from the nucleus [Fig. 1(e)].

A similar phenomenon is observed during cell division [Fig. 1(b)], i.e., in metaphase, where the fluorescence in the mitotic spindle region is about 15%–20% higher than in the surrounding [see Figs. 1(d) and 1(f)]. This finding is somewhat surprising since the complete breakdown of the nuclear envelope in prometaphase has merged the initially separated cytoplasm and nucleoplasm into a contiguous fluid. It therefore seems that the spindle region maintains its distinct nucleuslike character even after nuclear envelope breakdown. This observation and its interpretation corroborate similar findings in nematode and insect cells where an accumulation of free tubulin in the vicinity of chromatin has been reported during metaphase [13,14].

Since EGFP is biochemically inert and has no localization signal, the apparently unbalanced distribution of EGFP seen in interphase and metaphase cells demands an explanation. One might argue that an immobilized pool of EGFP molecules, being associated with decondensed chromatin, tops up the freely mobile protein pool and hence leads to an elevated nuclear fluorescence. Yet, this reasoning cannot be sustained for metaphase cells in which chromatin is condensed and rather excludes EGFP [cf. Fig. 1(b)]. Moreover, bleaching EGFP molecules in the nucleus of Cos7 and HEK293 cells and monitoring the fluorescence recovery due to an exchange with the cytoplasmic pool, monoexponential recovery curves were observed with the characteristic times being indistinguishable from the timescales for the loss of cytoplasmic fluorescence [15]. We have repeated these experiments in HeLa

cells and our results confirmed monoexponential recovery and loss curves with virtually identical characteristic times, eventually resuming the initial steady-state fluorescence ratio. This finding supports the notion of two well mixed compartments that exchange material by a one-dimensional diffusion process. It contrasts, however, with higher-order recovery curves that are expected if diffusion or binding processes within the cytoplasm and/or nucleoplasm were relevant for the exchange. In fact, it has been reported for various cell lines, including HeLa, that EGFP and similar macromolecules can cross the nuclear envelope by passive diffusion with the one-dimensional transit through nuclear pores being the rate-limiting step [15–19]. This transit is about tenfold slower than diffusion within the compartments [17], while diffusion of nanoscale particles within the nucleoplasm and cytoplasm of various cell lines, including HeLa, is very similar [20,21]. Hence, irrespective of the particular cell line, nucleoplasm and cytoplasm can be regarded as being almost well mixed during the rate-limiting diffusive exchange of EGFP between the nucleus and cytoplasm via nuclear pores. Therefore, the aforementioned finding of monoexponental recovery curves for the nuclear fluorescence [15] in combination with a fast restoration to prebleach fluorescence ratios gives good evidence that it is not an immobilized EGFP pool that leads to an elevated nuclear fluorescence.

An alternative and actually more straightforward explanation for the apparently nonuniform distribution of EGFP between compartments is a difference in their average accessible volume fraction $\langle\varphi\rangle$: If voxels in the nucleus are less crowded with inaccessible subvolumes on scales below the diffraction limit than their cytoplasmic counterparts, then the number of EGFP molecules is on average higher in nucleoplasmic voxels, leading to an elevated fluorescence. The same reasoning can be applied to the mitotic spindle region and its periphery when assuming these regions to maintain a different crowding even though a separating nuclear envelope is missing. As a consequence, the steady-state fluorescence of nucleus and spindle region are elevated when imaging within the linear range of excitation and detection, in line with our experimental observations (Fig. 1). Since illumination and detection settings are the same for both compartments within a single cell, the ratio of average fluorescence values between the two communicating compartments can be used to estimate their ratio of average accessible volume fractions, i.e.,

$$r = \begin{cases} \frac{\langle F_N\rangle}{\langle F_C\rangle} = \frac{\langle\varphi_N\rangle}{\langle\varphi_C\rangle} & \text{interphase,} \\ \frac{\langle F_S\rangle}{\langle F_P\rangle} = \frac{\langle\varphi_S\rangle}{\langle\varphi_P\rangle} & \text{metaphase} \end{cases} \tag{2}$$

with indices C, N, S, and P indicating cytoplasm, nucleoplasm, spindle region, and spindle periphery, respectively.

Indeed, the PDF of this ratio shows a distinct peak at $r > 1$ for ensembles of interphase and metaphase cells (Fig. 3), indicating that the accessible volume fraction in the nucleus is on average about 20% larger than in cytoplasm, and about 10% higher in the spindle region versus its periphery. In other words, the cytoplasm and the spindle periphery appear more crowded with inaccessible subvolumes than the nucleoplasm and spindle region, respectively. This slightly counterintuitive finding, i.e., a lower crowdedness in the nucleus, has already been suggested earlier by a significant difference of the diffusion anomaly in both compartments [20]. Moreover, in line with previous findings [13,14], our result suggests that the spindle region should be viewed as a compartmentlike entity with a distinct crowdedness albeit being contiguous with the previous cytoplasm.

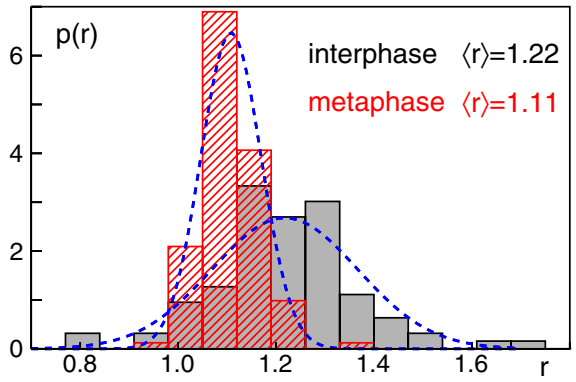

FIG. 3. The PDF of fluorescence ratios $p(r)$ obtained for cell ensembles in interphase (90 cells, gray histogram) and in metaphase (116 cells, red-hatched histogram) highlight an increased mean fluorescence in the nucleus (spindle) versus the surrounding cytoplasm (periphery). For each interphase cell, the ratio r of the mean fluorescence in the nucleus and in the cytoplasm was used; in metaphase cells the ratio employed the mean fluorescence in the spindle region as compared to its periphery. Treatment of interphase cells with nocodazole did not significantly change the ratio r, therefore, these data were included into the ensemble of interphase cells. Dashed blue lines are Gaussians with the mean and variance given by the experimental data, highlighting a significant deviation of the mean ratio $\langle r\rangle$ from unity.

Inspecting $p(r)$ for interphase and metaphase cells more closely, a markedly higher width is apparent for interphase cells. In other words, the ratio of nucleoplasmic and cytoplasmic fluorescence varies considerably more than the corresponding ratio of spindle and periphery, hinting at an elevated crowding heterogeneity in at least one of these compartments. The next subsection is therefore devoted to quantifying compartment-intrinsic heterogeneities.

B. Spatial heterogeneity within compartments

So far, the focus was on differences in the apparent crowdedness between two distinct compartments, quantified via changes in the mean fluorescence [Eq. (2)]. But also within each compartment one may expect some heterogeneity in the crowdedness. To explore this compartment-specific heterogeneity we have employed the coefficient of variation, i.e., the ratio of the standard deviation and the mean, which reads as, for any observable x,

$$\eta(x) = \frac{\sigma(x)}{\langle x\rangle} . \tag{3}$$

As a first step, we have focused on quantifying the heterogeneity within a compartment on intermediate length scales. To this end, we have selected for each interphase cell 20 regions of interest (ROIs) in cytoplasm and in the nucleus, with each ROI containing $N_v \approx 500$ voxels. The same was repeated for metaphase cells with 8 and 12 regions inside and outside

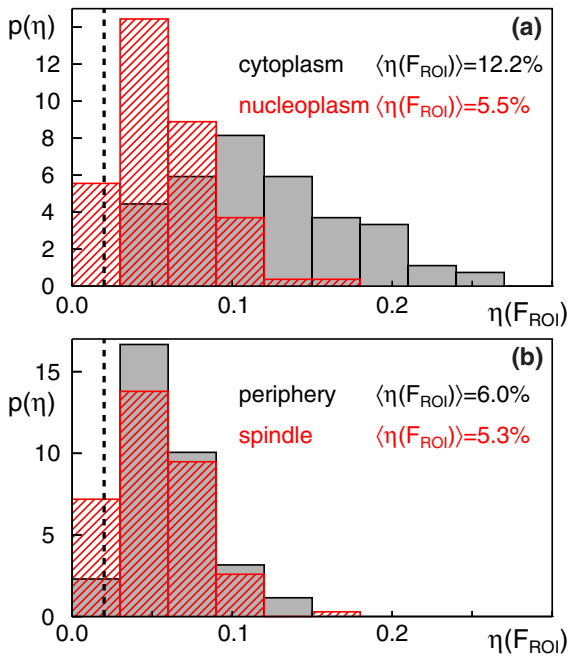

FIG. 4. (a) The PDF of the compartment-specific regional fluorescence heterogeneity $\eta(F_{\mathrm{ROI}})$, which is used as a proxy for the heterogeneity of the regional accessible volume fraction $\eta(\varphi)$ on intermediate length scales, shows marked differences between cytoplasm and nucleoplasm. (b) In contrast, little to no differences are visible for the crowding heterogeneity in the spindle region and its periphery in an ensemble of metaphase cells. Dashed vertical lines indicate the significance limit. See also main text for discussion.

the spindle area, respectively. Then, we calculated for each individual ROI the voxels' mean fluorescence $F_{\mathrm{ROI}} = \langle F \rangle_{\mathrm{ROI}}$ and its variance $\sigma^2(F) = \langle (F - F_{\mathrm{ROI}})^2 \rangle_{\mathrm{ROI}}$. In addition, we calculated for each cell and compartment the standard deviation $\sigma(F_{\mathrm{ROI}})$ of the mean fluorescence in the respective ensemble of ROIs. Using $\sigma(F_{\mathrm{ROI}})$ and F_{ROI} in Eq. (3) yields $\eta(F_{\mathrm{ROI}})$ which is a proxy for the compartment's heterogeneity of the accessible volume fraction $\eta(\varphi)$ on a length scale of several microns since $F_{\mathrm{ROI}} \propto \langle \varphi \rangle_{\mathrm{ROI}}$.

As a result, we observed that the PDF of $\eta(F_{\mathrm{ROI}})$ was spread over the interval $0 \leqslant \eta(F_{\mathrm{ROI}}) \leqslant 20\%$ for all compartments with average heterogeneities in the range of 5%–10% (Fig. 4). As anticipated from mere visual impressions [cf. images in Figs. 1(a) and 1(b)], the cytoplasm was indeed more heterogeneous than the nucleoplasm, the spindle region, or the spindle periphery. Therefore, on length scales of the chosen ROIs the cytoplasm features a roughly twofold higher crowding heterogeneity than the nucleoplasm. These crowding heterogeneities did not change significantly throughout interphase. Interestingly, virtually no change in the crowding heterogeneity was seen when comparing the nucleoplasm in interphase with the spindle region and/or its periphery in metaphase cells. Thus, while the overall crowding state differed markedly between compartments (cf. Fig. 3), compartment-intrinsic heterogeneities of nucleoplasm, spindle, and periphery are virtually the same.

Let us now briefly discuss in which regime values for $\eta(F_{\mathrm{ROI}})$ can be deemed significant. Given that F_{ROI} fluctuates to some extent even for homogeneous samples, a lower cutoff is needed above which the heterogeneity $\eta(F_{\mathrm{ROI}})$ can be used as a meaningful measure for the spatial heterogeneity. As a first estimate for this lower bound we have chosen the relative standard error for an individual region's mean fluorescence $\sigma(F)/(\sqrt{N_v} F_{\mathrm{ROI}})$. While this number varied slightly between regions, it was on average about 1% for all compartments and cells. This suggests that all values $\eta(F_{\mathrm{ROI}}) > 0.01$ may be deemed significant. A second estimate was obtained by repeating the evaluation approach for $\eta(F_{\mathrm{ROI}})$ with 20 ROIs using a set of images obtained for homogeneous samples like dye solutions or autofluorescent plastic slides (Chroma). As a result of these experiments, we found that these homogeneous samples feature a mean heterogeneity $\langle \eta(F_{\mathrm{ROI}}) \rangle_{\mathrm{hom}} \leqslant 2\%$, consistent with but slightly larger than our first estimate. We have therefore chosen the 2% level as a lower boundary for significant values of the spatial heterogeneity. In comparison to this boundary, the vast majority of data and all mean heterogeneities $\langle \eta(F_{\mathrm{ROI}}) \rangle$ are significant (cf. Fig. 4), indicating that the mesoscale heterogeneity of the accessible volume fraction is indeed 5%–10% for the examined compartments.

Going beyond intermediate length scales, we also aimed at resolving the voxel-wise heterogeneity within individual compartments. Since the variance of fluorescence values $\sigma^2(F)$ does not directly reflect the variance of the local accessible volume fraction $\sigma^2(\varphi)$ (see Material and Methods section), gaining insights on this shortest length scale is somewhat challenging. Employing the data obtained for the previously used ROIs, one can express the variance of fluorescence values F within each region as

$$\sigma^2(F) = \beta^2 [F_{\mathrm{ROI}} + A^2 \sigma^2(\varphi)], \tag{4}$$

where $F_{\mathrm{ROI}} = A\varphi_0$ is determined via the local mean accessible volume fraction φ_0 and $A^2\sigma^2(\varphi)$ reflects the location-dependent variation of the accessible volume fraction. While both F_{ROI} and $A^2\sigma^2(\varphi)$ vary between different ROIs within the same compartment of an individual cell, all imaging conditions are unchanged, i.e., the parameters β^2 and A remain constant. Moreover, for each of these ROIs the value of $A^2\sigma^2(\varphi)$ will only deviate randomly and unbiased from the mean over all ROIs $\langle A^2\sigma^2(\varphi) \rangle_{\mathrm{ROI}}$. Therefore, one can extract the unknown prefactor β^2 by fitting the data pairs $(F_{\mathrm{ROI}}, \sigma^2(F))$ for all ROIs within the same compartment of a single cell with a simple linear function. As a result of this fit process, one can estimate the voxel-wise heterogeneity of the accessible volume fraction for each ROI with the help of Eq. (4) as

$$\eta(\varphi) = \frac{A\sigma(\varphi)}{A\varphi_0} = \frac{\sqrt{\sigma^2(F)/\beta^2_{\mathrm{fit}} - F_{\mathrm{ROI}}}}{F_{\mathrm{ROI}}} = \eta(F). \tag{5}$$

Following this approach, we observed that cytoplasm, nucleoplasm, spindle, and periphery feature similar crowding heterogeneities on the level of individual voxels (Fig. 5), with a tendency of higher heterogeneities in cytoplasm and periphery as found already for larger length scales (cf. Fig. 4). Again, the crowding heterogeneity was not seen to change throughout interphase. As before, we estimate the lower bound for a significant heterogeneity to be about 2%. Given that the data are consistent with the previous, region-focused approach, it

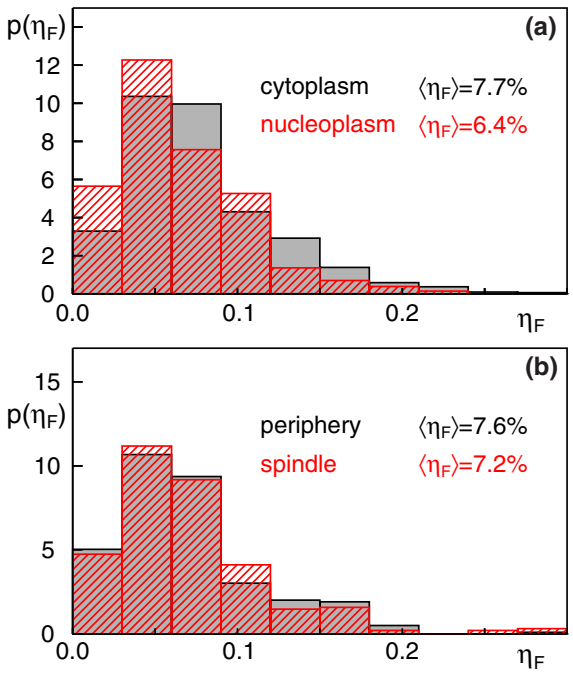

FIG. 5. The PDF of the voxel-wise heterogeneity $\eta(F)$ [see Eq. (5) and main text for details] indicates a similar heterogeneity of the accessible volume fraction for (a) cytoplasm and nucleoplasm, and for (b) the spindle region and its periphery.

appears reasonable to assign all compartments a local, voxel-wise heterogeneity of about 7%. We would like to emphasize, however, that this number is more vague than our above results since the evaluation approach includes a fitting process with relatively few data points which may introduce additional fluctuations.

Having obtained now some quantitative insights into the compartment-specific crowding heterogeneity in living cells, we would like to relate our findings to previous data. Experiments on quantifying the spatial heterogeneity of anomalous diffusion, i.e., quantifying the crowding-induced anomaly exponent α at different loci, had revealed $\eta(\alpha) \approx 8\%$ in cytoplasm and nucleoplasm [11]. At first glance, our findings of $\eta(\varphi) \sim 7\%$ on the smallest length scale (Fig. 5) seem to compare favorably to these observations. Yet, translating $\eta(\alpha)$ to $\eta(\varphi)$ had suggested a threefold to fourfold higher value for $\eta(\varphi)$ than measured in this study. We speculate that this deviation is due to two reasons: First, the approximations needed for the translation $\eta(\alpha) \to \eta(\varphi)$, e.g., the simple scaling $\varphi \propto 1 - \alpha$, may need some refinement. For example, including a critical threshold for φ below which an anomalous diffusion emerges in the first place, can reduce the apparent discrepancy between the two measurement approaches about twofold. Second, $\eta(\alpha)$ reports on the dynamical consequences of crowding whereas $\eta(\varphi)$ only reflects mere excluded-volume effects. Given that nonspecific interactions can tune the diffusion anomaly at constant accessible volume fractions [22,23], some discrepancy between our current data and complementary dynamical measurements may be expected. Finally, the relation $\eta(\varphi) \approx \eta(F)$, used here at several instances, is certainly also an approximation. Despite these limitations, our data on the compartment-specific heterogeneity of intracellular fluids provides an assessment that does not require transport measurements. Hence, our data complement previous insights and they are likely to be a useful starting point for simulation approaches of complex intracellular media and a deeper understanding of the emergence of heterogeneous diffusion processes in complex biological media.

ACKNOWLEDGMENT

Financial support by the VolkswagenStiftung (Grant No. Az. 92738) is gratefully acknowledged.

[1] H. Zhou, G. Rivas, and A. Minton, Annu. Rev. Biophys. **37**, 375 (2008).
[2] B. Alberts, *Molecular Biology of the Cell*, 6th ed. (Garland Science, New York, NY, 2015).
[3] J. Dix and A. Verkman, Annu. Rev. Biophys. **37**, 247 (2008).
[4] F. Höfling and T. Franosch, Rep. Prog. Phys. **76**, 046602 (2013).
[5] M. Weiss, Int. Rev. Cell Mol. Biol. **307**, 383 (2014).
[6] B. Wang, J. Kuo, S. C. Bae, and S. Granick, Nat. Mater. **11**, 481 (2012).
[7] P. Massignan, C. Manzo, J. A. Torreno-Pina, M. F. García-Parajo, M. Lewenstein, and G. J. Lapeyre, Jr., Phys. Rev. Lett. **112**, 150603 (2014).
[8] T. J. Lampo, S. Stylianidou, M. P. Backlund, P. A. Wiggins, and A. J. Spakowitz, Biophys. J. **112**, 532 (2017).
[9] T. Kuhn, T. O. Ihalainen, J. Hyvaluoma, N. Dross, S. F. Willman, J. Langowski, M. Vihinen-Ranta, and J. Timonen, PLoS One **6**, e22962 (2011).
[10] P. Struntz and M. Weiss, J. Phys. D: Appl. Phys. **49**, 044002 (2016).
[11] O. Stiehl and M. Weiss, Soft Matter **12**, 9413 (2016).
[12] N. Pawar, C. Donth, and M. Weiss, Curr. Biol. **24**, 1905 (2014).
[13] H. Hayashi, K. Kimura, and A. Kimura, Mol. Biol. Cell **23**, 1688 (2012).
[14] N. Schweizer, N. Pawar, M. Weiss, and H. Maiato, J. Cell Biol. **210**, 695 (2015).
[15] X. Wei, V. G. Henke, C. Strubing, E. B. Brown, and D. E. Clapham, Biophys. J. **84**, 1317 (2003).
[16] P. L. Paine, L. C. Moore, and S. B. Horowitz, Nature (London) **254**, 109 (1975).
[17] D. Mohr, S. Frey, T. Fischer, T. Guttler, and D. Gorlich, EMBO J. **28**, 2541 (2009).
[18] K. Ribbeck and D. Gorlich, EMBO J. **20**, 1320 (2001).
[19] B. L. Timney, B. Raveh, R. Mironska, J. M. Trivedi, S. J. Kim, D. Russel, S. R. Wente, A. Sali, and M. P. Rout, J. Cell Biol. **215**, 57 (2016).
[20] G. Guigas, C. Kalla, and M. Weiss, Biophys. J. **93**, 316 (2007).
[21] G. Guigas, C. Kalla, and M. Weiss, FEBS Lett. **581**, 5094 (2007).
[22] O. Stiehl, K. Weidner-Hertrampf, and M. Weiss, Phys. Rev. E **91**, 012703 (2015).
[23] F. Etoc, E. Balloul, C. Vicario, D. Normanno, D. Lisse, A. Sittner, J. Piehler, M. Dahan, and M. Coppey, Nat. Mater. **17**, 740 (2018).